Kinome Profiling in Pediatric Brain Tumors as a New Approach for Target Discovery

Arend H. Sikkema,[1] Sander H. Diks,[2] Wilfred F.A. den Dunnen,[3] Arja ter Elst,[1] Frank J.G. Scherpen,[1] Eelco W. Hoving,[4] Rob Ruijtenbeek,[5] Piet J. Boender,[5] Rik de Wijn,[5] Willem A. Kamps,[1] Maikel P. Peppelenbosch,[2] and Eveline S.J.M. de Bont[1]

Departments of [1]Pediatric Oncology, [2]Cell Biology, [3]Pathology and Medical Biology, and [4]Neurosurgery, University Medical Center Groningen, University of Groningen, Groningen, The Netherlands and [5]PamGene International B.V., Hertogenbosch, The Netherlands

Abstract

Progression in pediatric brain tumor growth is thought to be the net result of signaling through various protein kinase-mediated networks driving cell proliferation. Defining new targets for treatment of human malignancies, without *a priori* knowledge on aberrant cell signaling activity, remains exceedingly complicated. Here, we introduce kinome profiling using flow-through peptide microarrays as a new concept for target discovery. Comprehensive tyrosine kinase activity profiles were identified in 29 pediatric brain tumors using the PamChip kinome profiling system. Previously reported activity of epidermal growth factor receptor, c-Met, and vascular endothelial growth factor receptor in pediatric brain tumors could be appreciated in our array results. Peptides corresponding with phosphorylation consensus sequences for Src family kinases showed remarkably high levels of phosphorylation compared with normal tissue types. Src activity was confirmed applying Phos-Tag SDS-PAGE. Furthermore, the Src family kinase inhibitors PP1 and dasatinib induced substantial tumor cell death in nine pediatric brain tumor cell lines but not in control cell lines. Thus, this study describes a new high-throughput technique to generate clinically relevant tyrosine kinase activity profiles as has been shown here for pediatric brain tumors. In the era of a rapidly increasing number of small-molecule inhibitors, this approach will enable us to rapidly identify new potential targets in a broad range of human malignancies. [Cancer Res 2009;69(14):5987–95]

Introduction

Cancers arise by an evolutionary process as somatic cells mutate and escape the restraints that normally withhold them from unlimited expansion. To forestall unlimited cell division, multiple mechanisms work in concert. Neoplastic progression is the net result of uncontrolled signaling through various protein kinase-mediated networks driving cell proliferation. In neoplasms, cell signaling involving these pathways can be affected by numerous factors: genetic, epigenetic, and environmental (1). In theory, these signals converge into a limited number of downstream effectors. The most prominent signal transduction pathways implicated to mediate these growth and suppressive signals include the Janus-activated kinase/Stat, phosphatidylinositol 3-kinase/Akt, and Ras/extracellular signal-regulated kinase and protein kinase Cα pathways (2). In pediatric brain tumors, research mainly focused on the potential involvement of specific protein kinases such as epidermal growth factor receptor, platelet-derived growth factor receptor, phosphatidylinositol 3-kinase, and Janus-activated kinase in cell proliferation and survival (3–8). The overall complexity and coregulation of the various signaling networks, however, has not been unraveled yet. Therefore, high-throughput procedures, such as kinome profiling, which generates comprehensive insight in cellular signaling without *a priori* assumptions, would enable us to directly assess a broader range of targets for future treatment strategies.

Microarray-based kinome profiling approaches have been subject of development over the last years (9–13). In the present study, this approach has been employed for the detection of aberrant kinase activity in neoplastic tissue for the first time. Global tyrosine kinase activity profiles of pediatric brain tumors were identified applying a newly developed peptide array system (PamGene; ref. 14).

In the PamChip tyrosine kinase profiling system, a sample is constantly pumped up and down through a porous microarray of 144 kinase substrates. The phosphorylation is determined by measuring the association of a fluorescently labeled anti-phosphotyrosine antibody to the substrates phosphorylated by the kinase activities in the sample.

This procedure generated a comprehensive set of kinase-induced peptide phosphorylation profiles of all tumor samples included in this study. Peptide array data were validated by a combination of conventional and state-of-the-art techniques, such as cell survival assays and Phos-Tag SDS-PAGE, thereby establishing Src kinase as a primary target for therapeutic intervention in pediatric brain tumors.

The results show the usefulness of kinase activity profiling as a powerful approach to identify new potential targets for treatment.

Materials and Methods

Patient samples and cell lines. All tissue was obtained by surgical resection. After resection, the tissue was subjected to a short period of room temperature to transfer the tissue from operation room to the pathology department (mean time, 10 min). Subsequently, the tissue samples were snap frozen in liquid nitrogen and stored at −80°C.

Tissue material was histologically evaluated and graded according to WHO classification 2007 (15). Written informed consent and local ethics committee approval was granted for use of the patient material.

Tyrosine kinase activity profiles of 29 pediatric brain tumors (9 ependymomas, 7 pilocytic astrocytomas, and 13 primitive neuroectodermal tumors, of which 10 medulloblastomas) were generated

Note: Supplementary data for this article are available at Cancer Research Online (http://cancerres.aacrjournals.org/).

Requests for reprints: Eveline S.J.M. de Bont, Department of Pediatric Oncology, University Medical Center Groningen, University of Groningen, Hanzeplein 1, 9713 GZ Groningen, The Netherlands. Phone: 31-50-3614146; Fax: 31-50-3611671; E-mail: e.de.bont@bkk.umcg.nl.

doi:10.1158/0008-5472.CAN-08-3660

(Supplementary Table S1). Wilms' tumor (n = 5) and colon carcinoma (n = 5) tissue was included to study tumor specificity. Normal kidney (n = 2) and colon tissue (n = 5) samples were included as control tissue.

We used the cell lines Uw-402, Uw-426, Uw-473, Res-256 (medulloblastoma), Res-186, Res-259, Uw-467 (low-grade astrocytoma) Res-196 (ependymoma; Dr. Michael S. Bobola, Seattle Children's Hospital Research Institute), DAOY (medulloblastoma), DLD-1 (colon carcinoma), 293T (human embryonic kidney), TF-1 (acute myeloid leukemia), K-562 (chronic myeloid leukemia; American Type Culture Collection), and HL-60 (acute myeloid leukemia; German Collection of Microorganisms and Cell Cultures). DAOY and 293T were cultured in DMEM (Lonza) supplemented with 10% fetal bovine serum (Bodinco). The other brain tumor cell lines were cultured in DMEM/F-12 (Invitrogen) containing 5% fetal bovine serum. HL-60, TF-1, and DLD-1 were grown in RPMI 1640 (Lonza) with 10% fetal bovine serum. Cell cultures contained 100 units/mL penicillin and 100 μg/mL streptomycin (PAA Laboratories). Granulocyte/macrophage colony-stimulating factor (Novartis) was supplemented to the TF-1 cultures (10 ng/mL).

Tyrosine kinase activity profiling using PamChip peptide arrays. Kinase activity profiles were determined using the PamChip tyrosine kinase microarray system (PamGene). This microarray consists of 144 unique peptide sequences spotted onto a porous membrane enabling constant flow-through of the reaction mixture.[6] Each peptide represents a 15-amino acid sequence corresponding to a putative endogenous phosphorylation site, which functions as a tyrosine kinase substrate (Supplementary Table S2). Phosphorylation is visualized by measurement of the endpoint fluorescent signal emitted as a consequence of fluorescein-labeled anti-phosphotyrosine antibody binding (PY20).

Tissue was lysed in M-PER reagent containing phosphatase and protease inhibitors (Pierce). The reaction mixture consisted of 1× ABL buffer (Westburg), 100 μmol/L ATP (Sigma-Aldrich), 20 μg/mL PY20 (Exalpha), and 5 μL lysate. Before loading, the reaction mixture onto the array a blocking procedure was done with 0.2% bovine serum albumin (Calbiochem). The experiment was repeated 8 times for each tissue sample to study technical reproducibility. After loading the cell lysates onto the PamChip arrays, incubation was commenced for 60 cycles using the PamStation96 followed by washing and FITC fluorescence measurement of all peptide spots.

The optimal protein concentration was determined by adding samples with various protein concentrations to the array. Between 0.5 and 1.5 μg/μL, variation in the total amount of protein applied to the array did not influence signal intensity (data not shown). Protein concentrations were measured in the first experiments to standardize the tissue procedure (12 slices of 5 μm of a tissue block measuring 5 × 5 mm).

Tissue-Tek OCT compound (Sakura Finetek) used in the tissue freezing procedure did not affect kinase activity.

Immunoblotting of phosphorylated Src. The immunoblotting procedure was done basically as described previously (16). Frozen tissue was lysed in 250 μL radioimmunoprecipitation assay buffer containing Complete solution (Roche Diagnostics) and 1 mmol/L Na_3VO_4. Cultured cells were washed with ice-cold PBS and scraped in 500 μL radioimmunoprecipitation assay buffer. Laemmli sample buffer was supplemented and the lysate was boiled for 5 min.

To visualize the levels of phosphorylated Src, a newly developed immunoblotting technique was applied using a phosphate-binding molecule (Phos-Tag AAL-107; NARD Institute; ref. 17). Together with 0.2 mmol/L $MnCl_2(H_2O)_4$, 0.1 mmol/L Phos-Tag AAL-107 ligand was added to the SDS-PAGE (7.5%). Protein was blotted onto a polyvinylidene fluoride membrane (Millipore). Blots were incubated at 4°C in 5% bovine serum albumin containing a primary antibody against total Src (2 μg/mL stock; 1:1,000; 36D10 rabbit monoclonal antibody; Cell Signaling) overnight followed by incubation with swine anti-rabbit peroxidase-conjugated antibodies (1:3,000; P0217; DAKO) at room temperature for 1 h. Antibody binding was visualized by enhanced chemiluminescence. β-Actin was probed as a protein loading control (200 μg/mL stock; 1:3,000; sc-47778 mouse monoclonal antibody; Santa Cruz Biotechnology).

Cell survival assays. A WST-1 colorimetric viability assay protocol was done following the procedures recommended by the manufacturer (Roche). Cells were seeded at a density of 4×10^4 per well in medium (1% fetal bovine serum) and subjected to 0, 0.1, 0.5, 1, 2, and 20 μmol/L 4-amino-5-(4-methylphenyl)-7-(*t*-butyl)pyrazolo [3,4-*d*]pyrimidine (PP1; BioMol International) or 0, 0.05, 0.1, 0.5, 1, 5, 10, 50, and 100 nmol/L dasatinib (BMS-354825; Bristol Myers Squibb) for 48 h (6 replicates for each concentration).

Cell proliferation assays. 5-Bromo-2-deoxyuridine cell proliferation assays were done following the procedures recommended by the manufacturer (Merck Biosciences). Cells were seeded at a density of 2×10^4 per well and incubated with either 0, 2, or 20 μmol/L PP1 in medium containing 1% fetal bovine serum (6 replicates for each concentration). 5-Bromo-2-deoxyuridine was added after 0, 24, or 48 h incubation with PP1 followed by another 24 h of incubation.

Data analysis and statistics. Quantification of spot intensities was conducted using Bionavigator software (PamGene).

Background was determined by plotting all signals against the relative SE over the replicates. The threshold signal intensity was read from the trend line at an relative SE of 1/e (~ 37%), above which signals were considered to reflect a genuine phosphorylation event. Phosphorylation values with a relative SE exceeding 37% were excluded from further analysis. Data analysis was done in BRB-Array Tools version 3.5.0 (18). Data normalization was achieved by determining the median signal over each array. Differences in peptide phosphorylation were statistically assessed with nonparametric Mann-Whitney U tests in SPSS (release 14.0.2).

Differences in 5-bromo-2-deoxyuridine incorporation levels were statistically assessed with Kruskal-Wallis one-way ANOVA (SPSS).

The Phospho-ELM BLAST tool (Phosphobase Resource Release 7.0) was applied to determine the kinases potentially responsible for phosphorylation of a specific peptide.[7]

Results

Tyrosine kinase activity profiles of pediatric brain tumors. The flow-through feature of the PamChip tyrosine kinase profiling system resulted in a low and evenly distributed background signal, making it possible to measure kinase activity in high resolution. Measuring the signal intensities of highly phosphorylated peptides at multiple time points indicated that the phosphorylation signals did not reach the plateau during the run.

To study the reproducibility of the peptide array data, we generated kinome profiles in separate assay-runs on the same day and on separate days. Hierarchical clustering showed comparable lists of phosphorylation values in both cases. Furthermore, regression analysis comparing the phosphorylation values of identical patient tissue, prepared and analyzed on separate days, rendered a R2 value of 0.79 (Supplementary Fig. S1).

To determine the time window for measuring tyrosine kinase activity (time between tissue resection and freezing during operation), kinase activity profiles of tumor tissue lysed after either, 2, 5, 10, 20, or 30 min incubation at room temperature were established. No differences in kinase activity profiles were observed up until 30 min of room temperature with a R2 of 0.91 comparing the values after 2 and 30 min of incubation (Supplementary Fig. S2). Thus, we can conclude that kinase activity is sufficiently stable to allow analysis according to our experimental setup.

[6] www.PamGene.com

[7] http://phospho.elm.eu.org/pELMBlastSearch.html

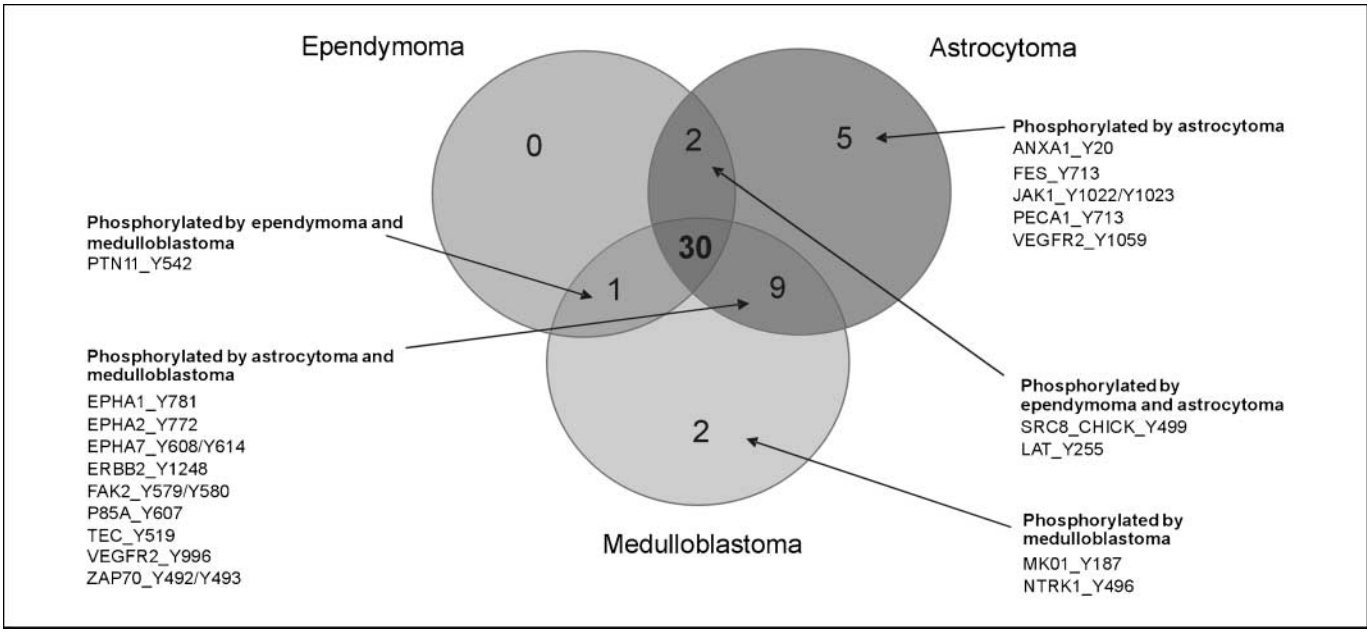

Figure 1. Peptides phosphorylated by astrocytoma, medulloblastoma, and ependymoma tissue lysate. The number and identity of the peptides phosphorylated by >90% of the samples within one tumor type are displayed in a Venn diagram comparing peptide phosphorylation between the different pediatric brain tumor types. Forty-nine of the 144 peptides present on the array displayed signal intensities above the threshold value. A remarkable 30 peptides were phosphorylated by >90% of each type of pediatric brain tumor, whereas peptides preferentially phosphorylated by lysate of a specific tumor type can be appreciated as well.

Next, kinase activity profiles of pediatric brain tumor lysates were established. We used two methods to analyze the phosphorylation data. First, phosphorylation intensities of the peptides were compared between the different brain tumor subtypes in accordance with the minimal kinome approach described by Diks and colleagues (Fig. 1; ref. 19). The minimal kinome approach determines the set of substrates, the phosphorylation of which is shared by >90% of all samples within one tumor type. The central nervous system primitive neuroectodermal tumor samples were excluded from this analysis. Second, differences in phosphorylation levels were assessed by class comparison.

On average, the ependymoma, astrocytoma, and medulloblastoma tumor lysates elicited phosphorylation of 70, 73, and 72 peptides, respectively (Fig. 2; Supplementary Table S3). Phosphorylation of 30 substrates appeared to be common to all pediatric brain tumor types. Within this set of 30 peptides (Supplementary Table S4), suggested to represent the minimal tyrosine kinome of pediatric brain tumors within the current set of substrates, high levels of kinase activity were observed on peptides corresponding with phosphorylation consensus sequences derived from ERBB2/HER-2 receptor and c-Met/hepatocyte growth factor receptor kinases. Furthermore, with the aid of the Phospho-ELM database, we identified 20 peptides that could potentially be phosphorylated by Src family kinases. Seven of these peptides were present in the established minimal tyrosine kinome of pediatric brain tumors.

Differential phosphorylation of the vascular endothelial growth factor receptor 2 derived peptides was also observed. VEGFR2_Y1059 (DIYKDPDYVRKGD) was phosphorylated by all of the included medulloblastomas, whereas some ependymoma and astrocytoma samples lacked phosphorylation of this peptide. Furthermore, VEGFR2_Y996 (EEAPEDLYKDFLT) was phosphorylated by all astrocytomas and medulloblastomas but not all ependymomas.

Class comparison showed a significantly higher phosphorylation of the peptide LAT_Y200 (MESIDDYVNVPES) in astrocytomas compared with ependymomas. In addition, the phosphorylation of CBL_Y700 (EGEEDTEYMTPSS) by astrocytoma lysate was higher compared with medulloblastomas.

Overall, these results imply substantial overlap in kinase activity, whereas some phosphorylation events could be appreciated as potential druggable targets.

Tyrosine kinase activity profiles of neoplastic tissue and its normal counterpart. In the light of the observed similarities in kinase activity in three pediatric brain tumor types, we wondered whether these similarities are tumor specific. Therefore, we performed an experiment comparing kinase activity profiles of three diverse types of solid tumor. Kinase activity profiles of 9 pediatric brain tumors (A2, A6, A7, E2, E8, E9, M7, M8, and M9), 5 Wilms' tumors, and 5 colon carcinomas were compared with normal kidney (n = 2) and colon tissue (n = 5). Because there is no possibility of getting healthy normal brain tissue and postmortem brain tissue is not applicable due to the slow decrease in body temperature after death resulting in autolysis, we decided to compare the various brain tumor tissues with a small panel of normal tissues to see if the resolution of the technique is sufficient to discern differences in kinase activity. After data processing, 88 peptides showed signal intensities below the threshold value. Twenty-eight peptides, including substrates for Wee1, Src, Ret, Pak, and platelet-derived growth factor receptor-β, proved to be phosphorylated by lysate of all three tumor types (Fig. 3; Supplementary Table S4).

For the two tissue-normal counterpart combinations, the neoplastic tissue displayed a different number of phosphorylated peptides, reflecting altered tyrosine kinase activity in neoplastic cells. The colon carcinomas rendered an average of 75 phosphorylated peptides compared with 58 peptides applying normal colon tissue. For Wilms' tumors, this concerned 62 peptides compared with 66 in the normal kidney counterpart. Colon carcinoma lysate showed a

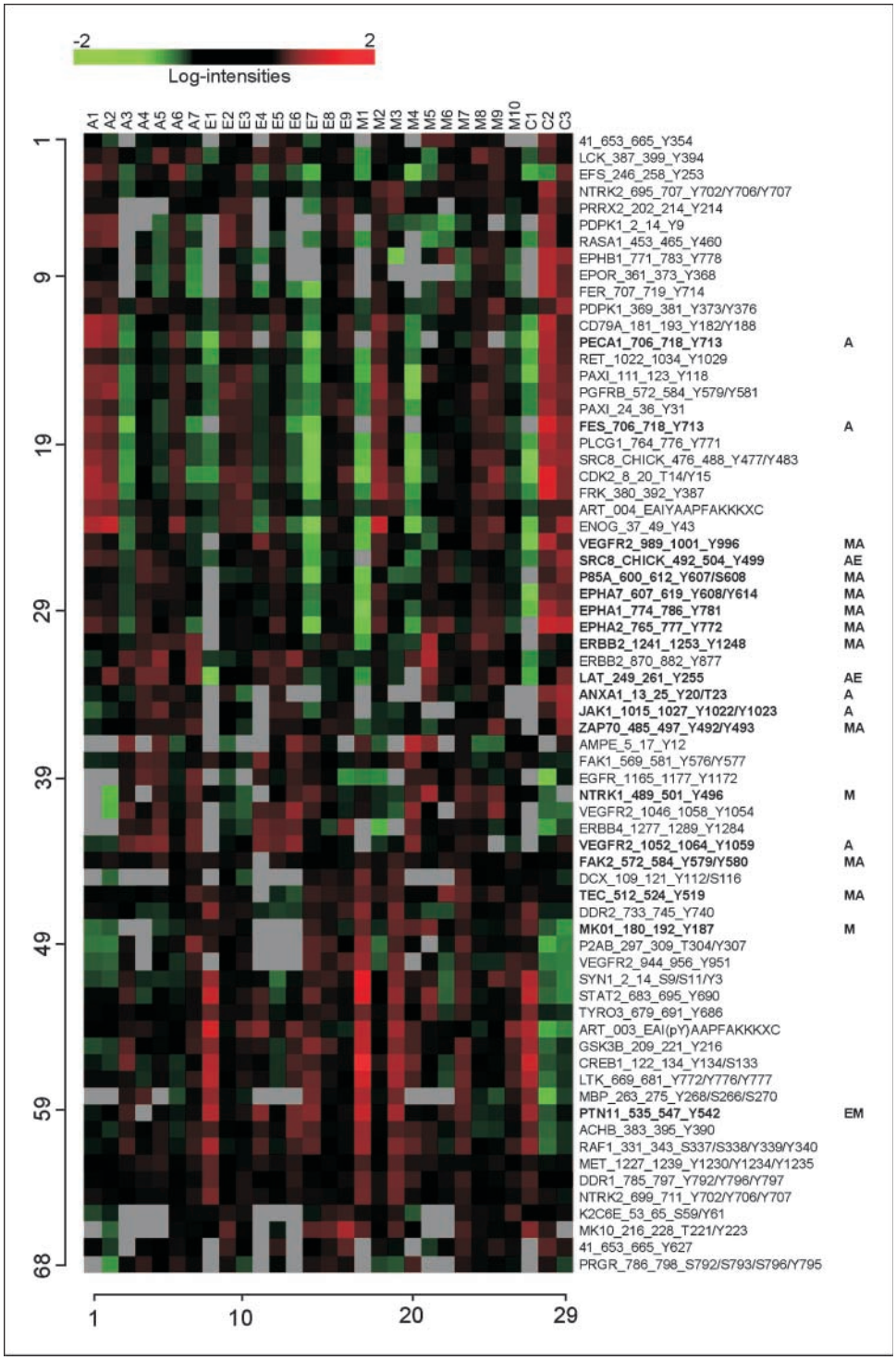

Figure 2. Supervised clustering of normalized peptide phosphorylation signals. The 68 peptides that were phosphorylated by >60% of all brain tumor lysates are displayed. *Red* and *green spots,* high and low signal intensities, respectively. Sample labels correspond with Supplementary Table S1. *A,* astrocytoma; *E,* ependymoma; *M,* medulloblastoma; *C,* central nervous system primitive neuroectodermal tumor. The peptide names correspond with the phosphorylation consensus sequences of the kinase from which they originated (Supplementary Table S2). *Bold,* peptides that are phosphorylated by >90% of the samples within one tumor type, as listed in Fig. 1.

significantly higher kinase activity on 5 peptide residues compared with normal counterpart tissue. These peptides correspond with consensus sequences of Src, Ret, and FAK tyrosine kinases.

Applying the minimal kinome approach, the colon and kidney tumors together produced unique phosphorylation of 11 peptides compared with 1 in their normal counterparts (Fig. 3). Within this set of 11 tumor-specific peptides, phosphorylation of CDK2_Y15 (EKIGEGTYGVVYK) and MET_Y1230/Y1234/Y1235 (RDMYDKEYYSVHN) can be appreciated. These peptides are also present in the established minimal pediatric brain tumor tyrosine kinome. Thus, although phosphorylation of a significant number of substrates is shared between tumors of different origin, also clear germ-line specific and tissue-specific phosphorylation patterns can be appreciated in cancers of different origin.

Differences in the phosphorylation status of Src-related peptides between pediatric brain tumor and normal tissue samples were assessed by class comparison. Interestingly, brain tumor lysate showed a significantly higher phosphorylation of 10 of the 20

potential Src substrates (Supplementary Fig. S3): ANXA1_Y20 (IENEEQEYVQTVK; P = 0.044), EFS_Y253 (GGTDEGIYDVPLL; P = 0.007), ENOG_Y43 (SGASTGIYEALEL; P = 0.005), P85A_Y607 (NENTEDQYSLVED; P = 0.012), PAXI_Y118 (VGEEEHVYSFPNK; P = 0.009), PAXI_Y31 (FLSEETPYSYPTG; P = 0.007), PDPK1_Y9 (ARTTSQLYDAVPI; P = 0.014), PDPK1_Y373/Y376 (DEDCYGNYDNLLS; P = 0.005), SRC8_CHICK_Y477/Y483 (EYEPETVYEVAGA; P = 0.016), and SRC8_CHICK_Y499 (YQAEENTYDEYEN; P = 0.009). These results imply Src activity to be a prominent characteristic of pediatric brain tumor growth.

Src-mediated signaling might be important in pediatric brain tumor progression. Src phosphorylation levels were determined in three tissue samples of each brain tumor type, applying the newly developed Phos-Tag SDS-PAGE approach. This technique makes use of the affinity of phosphorylated proteins for the Phos-Tag ligand, resulting in retention of phosphorylated proteins, separating them from their unphosphorylated counterpart during electrophoresis. In theory, this will result in two or more distinct protein bands representing the phosphorylated and unphosphorylated status of the protein. Src possesses two key phosphorylation sites determining activity: the stimulatory site Tyr^{416} and the inhibitory site Tyr^{527}. Phosphorylation of both tyrosine residues renders the enzyme hyperactive (20, 21). Thus, three possible phosphorylation states can be appreciated: non-phosphorylated, single-phosphorylated at Tyr^{527} or Tyr^{416}, and double-phosphorylated at both Tyr^{527} and Tyr^{416}. On the Phos-Tag gels, we observed all three phosphorylation states, confirming Src kinase activation in tissue samples of all three brain tumor types as well as in each of 9 pediatric brain tumor cell lines (5 medulloblastomas, 3 astrocytomas, and 1 ependymoma; Fig. 4). We observed a less active phosphorylation ratio of Src in the control cell lines HL-60, DLD-1, and 293T.

To verify the functional role of Src kinases in pediatric brain tumor growth, cell survival assays were done using dasatinib and PP1 as potent Src family kinase inhibitors.

PP1 induced a dose-dependent decrease in cell survival in all brain tumor cell lines with LC_{50} (50% decline in cell survival) concentrations ranging from 1.1 to 9.7 μmol/L (Fig. 5). This was in agreement with the concentrations necessary to inhibit Src kinase activity (data not shown). Hardly any decrease in cell survival was seen in two leukemic cell lines (HL-60 and TF-1; LC_{50} > 20 μmol/L), suggesting other pathways to take over cell survival signaling in these cell lines. A substantially lower response to PP1 was also found in the colon carcinoma cell line DLD-1 (LC_{50} > 20 μmol/L) and the human embryonic kidney cell line 293T (LC_{50} > 20 μmol/L).

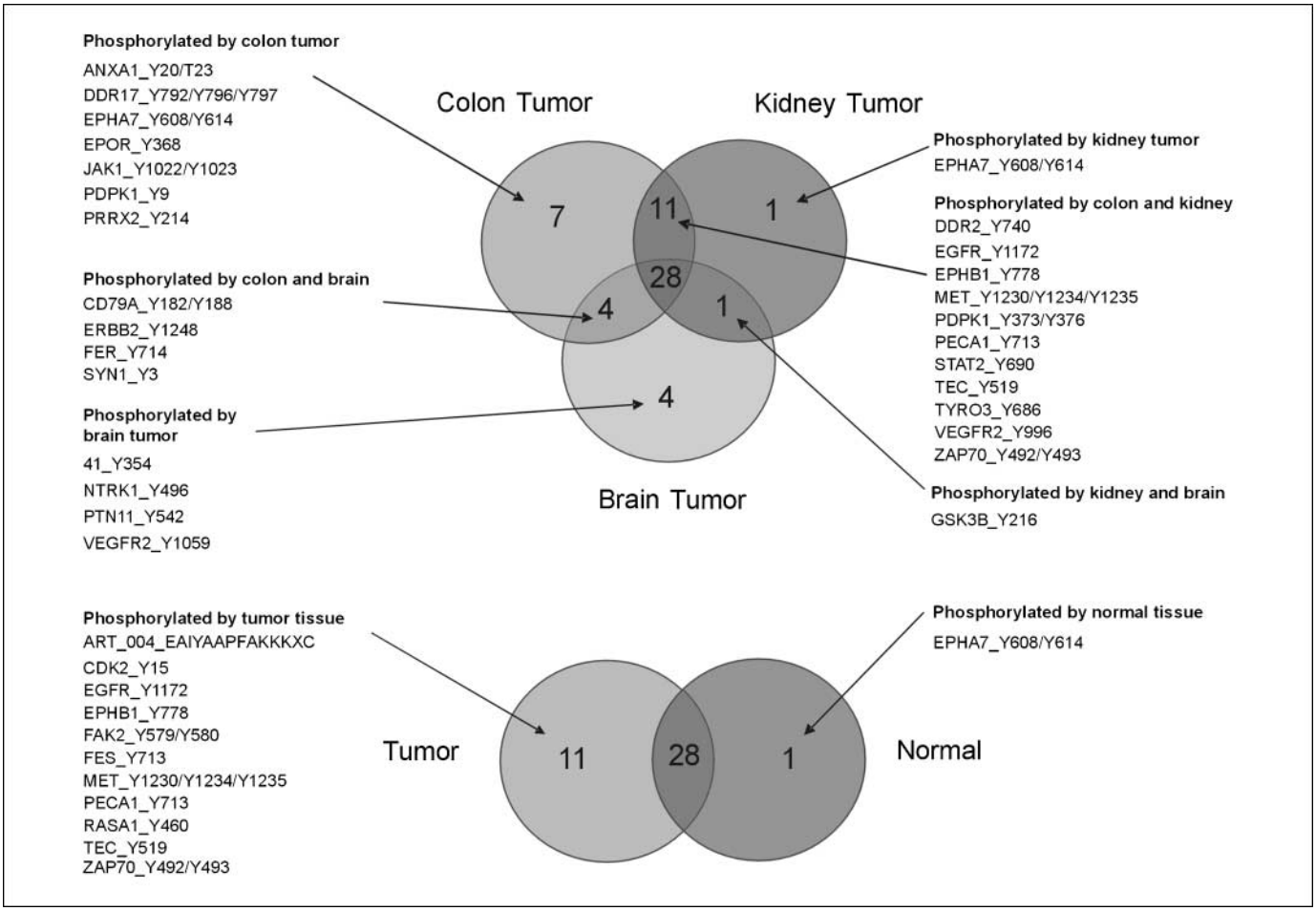

Figure 3. Tumor and tissue specificity of kinase activity profiles. Tyrosine kinase activity profiles of three diverse types of solid tumor were generated: colon carcinomas, Wilms' tumors, and pediatric brain tumors. Normal colon and kidney tissue were included as normal counterparts. The number and identity of the peptides phosphorylated by >90% of the samples within one tumor type are displayed in a Venn diagram. A list of peptides commonly phosphorylated by all three tumor types can be found in Supplementary Table S4. *Bottom,* Venn diagram of the peptides phosphorylated by either tumor or normal counterpart lysate. Forty peptides were phosphorylated by >90% of the tumor lysates, normal tissue samples, or both. Peptides preferentially phosphorylated by a specific tissue type are specified.

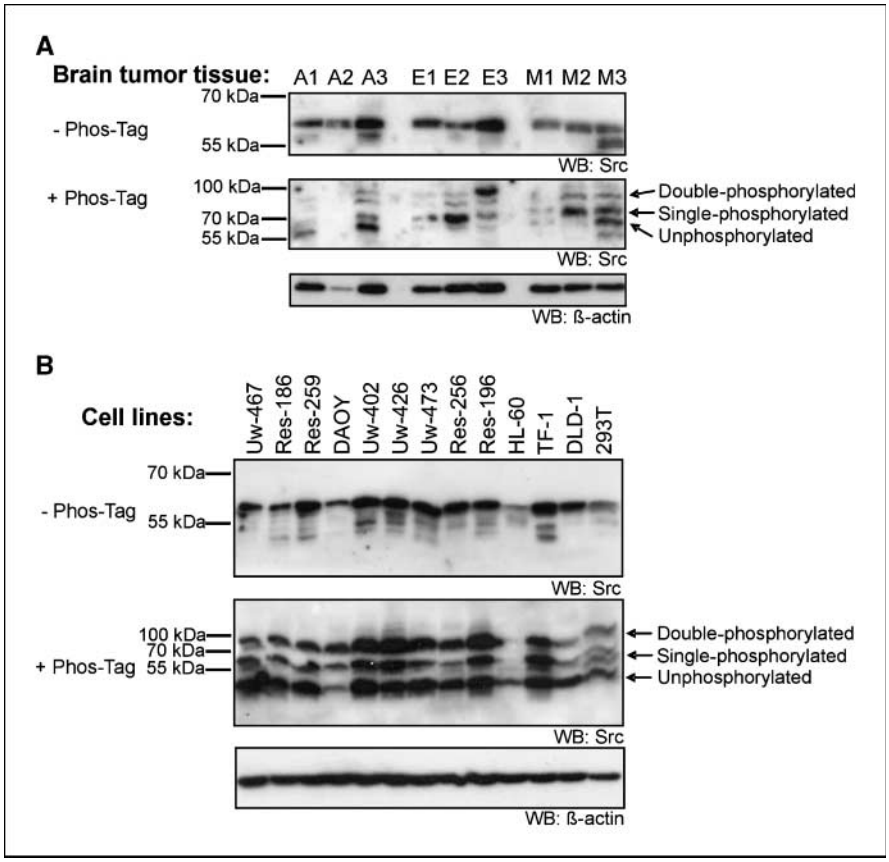

Figure 4. Phosphospecific SDS-PAGE confirms Src kinase activity. Src phosphorylation levels were determined in three tissue samples of each brain tumor type (*A*) and in each of the nine pediatric brain tumor cell lines [*B*; medulloblastoma (DAOY, Uw-402, Uw-426, Uw-473, and Res-256), astrocytoma (Res-186, Res-259, Uw-467), and ependymoma (Res-196)] using Phos-Tag SDS-PAGE. Phosphorylated proteins have affinity for the Phos-Tag ligand, resulting in separation of phosphorylated proteins from their unphosphorylated counterparts. On the Phos-Tag blots, three phosphorylation states representing unphosphorylated as well as single- and double-phosphorylated Src can be identified. Src kinase phosphorylated at both Tyr^{416} and Tyr^{527} renders a hyperactive isoform. Hence, the blotting results confirm substantial Src kinase activation. Although the expression of Src is lower in three of the four control cell lines (DLD-1, 293T, and HL-60), a lower ratio of active versus inactive Src can be observed. The phosphorylation status of Src in TF-1 is comparable with that of the pediatric brain tumor cell lines. Images have been cropped and background has been subtracted to improve clarity (see Supplementary Data for unaltered image).

Also, dasatinib decreased cell survival in all pediatric brain tumor cell lines, except for the low-grade astrocytoma cell line Uw-467 (Fig. 6). Three cell lines reached LC_{50} within the applied concentration range: Uw-473, Res-186, and Res-196 (65, 20, and 17 nmol/L, respectively). No effect could be observed on the control cell lines, except for the positive control K-562. The high apoptosis rate of K-562 on treatment with dasatinib is accompanied by an attenuation of the levels of phosphorylated Bcr-Abl, c-Src, Lyn, and CrkL, indicating that this effect is not only the result of Src inhibition in this specific cell line (22).

Summarizing, Src inhibitors are able to induce tumor cell death in pediatric brain tumor cell lines, whereas no effect can be observed in the controls.

The effect of Src inhibition on cell cycle arrest was determined by performing 5-bromo-2-deoxyuridine proliferation assays with the medulloblastoma cell line Uw-473 (Supplementary Fig. S4). Cell survival assays done in parallel indicated a strong dose-dependent decrease in Uw-473 cell survival with PP1 added ($P < 0.001$). A significant dose-dependent decrease in Uw-473 cell proliferation rate on Src inhibition was observed as well ($P < 0.01$).

Discussion

In this study, we successfully applied a novel high-throughput technique to generate tyrosine kinase activity profiles of pediatric brain tumors and show its usefulness in target discovery. We identified and validated Src activity as a potential target in pediatric brain tumors for therapeutic intervention.

The tyrosine kinase activity profiles of different pediatric brain tumor types showed considerable overlap. Using the minimal kinome approach, a set of 30 of 144 substrates proved to be phosphorylated in >90% of all brain tumor lysates. Eleven substrates showed tumor-specific activity in a comparison of various tumor tissues, such as pediatric brain tumors, Wilms' tumors, and colon carcinomas, with normal tissue types. Within these 11 tumor-specific substrates, CDK2, c-Met, and epidermal growth factor receptor-derived peptides were present.

The importance of CDK2 related to malignant progression has already been recognized. CDK2 is the major cell cycle kinase, which activation represents an increase in mitotic index (23–27). c-Met is the tyrosine kinase receptor of scatter factor/hepatocyte growth factor and has been shown to promote migration, invasion, and angiogenesis in gliomas followed by a decrease in prognosis (28–31). Interestingly, the scatter factor/hepatocyte growth factor/c-Met pathway has been shown to require CDK2 activation to induce cell cycle progression in medulloblastoma (32). The presented results suggest a more common role for c-Met-induced tumor progression involving CDK2 activation.

In all tumor types, substantial phosphorylation of several peptide motifs related to epidermal growth factor receptor family members was observed. Epidermal growth factor receptor signaling has been linked to various malignancies including childhood medulloblastoma (33, 34).

Summarizing, the observed tumor-specific kinase activity profile overlaps with previously published tyrosine kinase activation, proving the validity of the peptide array results. Moreover, this kinase activity profile is able to give us a view into the complexity and the subtlety of the cellular signaling networks that drive tumor cell proliferation in favor of tumor cell death.

On the peptide array, 20 potential Src substrates are present, of which 10 showed a significantly higher level of phosphorylation in

pediatric brain tumor tissues compared with normal tissues. With the aid of Phos-Tag SDS-PAGE, we were able to confirm an activatory phosphorylation status of Src in pediatric brain tumor lysates, whereas this was not the case in control cell types. The increased sensitivity of pediatric brain tumor cell lines, compared with several tumor control cell lines on increasing dosages of a Src family kinase inhibitor, points to a potentially important role of Src signaling in pediatric brain tumors. The successful application of Phos-Tag SDS-PAGE shows its potential in studying protein phosphorylation.

Src family kinases are controlled by various classes of receptor pathways including protein tyrosine kinases, integrin receptors, and G protein-coupled receptors. Src signals to a variety of downstream effectors including cytoskeletal proteins (FAK and paxillin) and pathways involving Stat, phosphatidylinositol 3-kinase, and extracellular signal-regulated kinase, thus exerting effects on cell survival, proliferation, and differentiation (35). We showed a decreased pediatric brain tumor cell viability and proliferation rate on Src inhibition. The LC_{50} concentrations of dasatinib were within nanomolar range. Dasatinib has been shown to decrease tumor cell survival and proliferation in breast cancer, non-small cell lung cancer, and neuroblastoma (36–39). Within the brain, Src family kinases are known to play a critical role in cerebellar cell migration and histogenesis during embryonic development (40–42). Recent publications have shown that Src signaling is also involved in brain tumor cell invasion. By preventing Src family kinase recruitment to epidermal growth factor receptor or CD95, a decrease in glioblastoma cell invasiveness could be established (43, 44). Furthermore, protein phosphatase activity of PTEN has been shown to control glioma cell migration by inhibition of Src family kinases (45). PTEN is mutated in one third of all glioblastomas. Our data provide the first evidence that Src signaling is an interesting potential target for pediatric brain tumor treatment. Preliminary data already showed that detectable concentrations of dasatinib can be reached in the cerebrospinal fluid (46).

Current mass spectrometry techniques and novel proteomics approaches such as antibody microarrays determine protein phosphorylation levels rather than the enzymatic activity resulting from it. Measurement of kinase activity using the peptide microarray provides a direct view on the extent of enzymatic activity leading to specific signal transduction. The validity of the PamGene tyrosine kinase array data has been studied previously by Lemeer and colleagues (47). They were able to confirm the peptide array phosphorylation data with anti-phosphotyrosine immunoprecipitation followed by mass spectrometry-based proteomics.

A potential drawback is the variation in the number of potential upstream kinases for the various substrates as determined using the Phospho-ELM database. In our view, the decreased kinase specificity of a peptide can be compensated by taking into account all substrates potentially sensitive to a kinase of interest, thereby enhancing the interpretability of the results. The annotation of

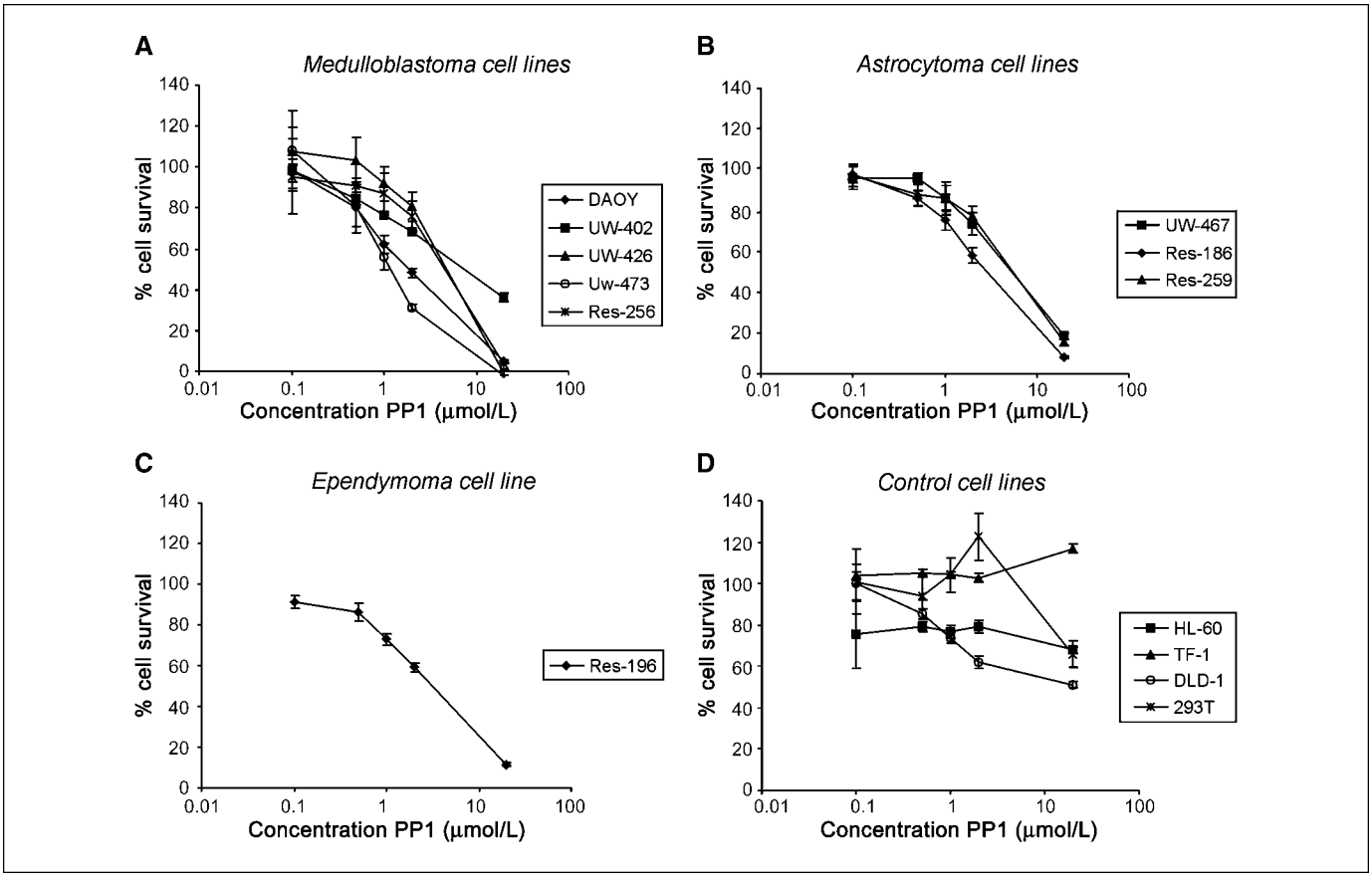

Figure 5. Decreased tumor cell survival in response to Src inhibition with PP1. Cell survival percentage has been plotted against the concentration of PP1 (μmol/L) for all medulloblastoma (*A*), astrocytoma (*B*), ependymoma (*C*), and control (*D*) cell lines. *Bars,* SD of six replicate measurements. All pediatric brain tumor cell lines show decreased cell survival.

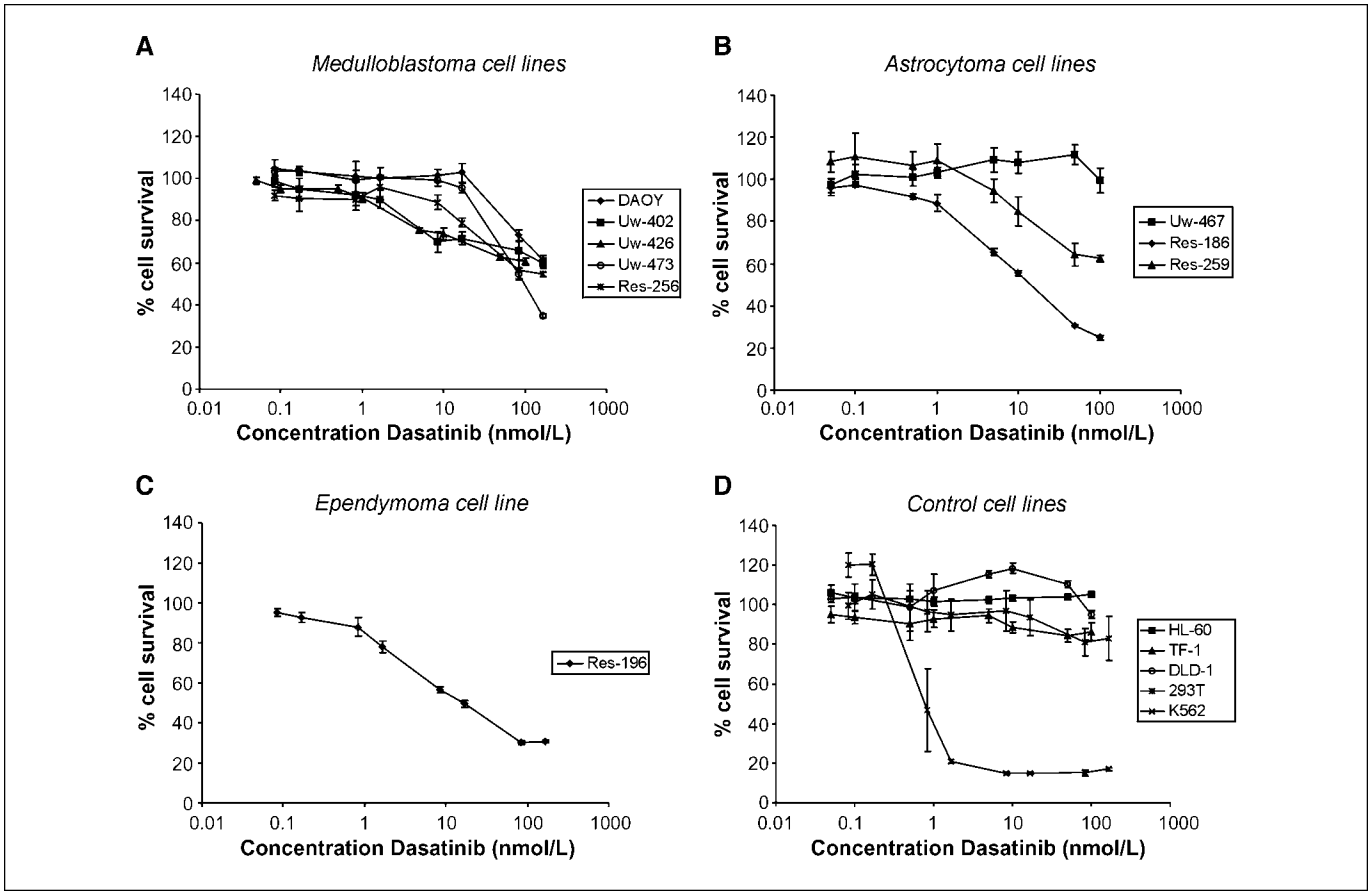

Figure 6. Decreased tumor cell survival in response to Src inhibition with dasatinib. Cell survival percentage has been plotted against the concentration of dasatinib (nmol/L) for all medulloblastoma (*A*), astrocytoma (*B*), ependymoma (*C*), and control (*D*) cell lines. The cell line K-562 functioned as a positive control. *Bars,* SD of six replicate measurements. With the exception of Uw-467, all pediatric brain tumor cell lines show decreased cell survival.

specific peptide substrates has gained reliability over the last years, as the Phospho-ELM database has expanded dramatically. Still, determining the sensitivity of a substrate for specific kinases will prove to be of tremendous value in future application of the peptide array. Most likely, future application of recombinant and/or purified kinases will tell us more about the specificity of individual peptides, thus making it easier to pinpoint specific kinases based on the obtained peptide array results. Therefore, generating hypotheses is the limit of what is possible at the current developmental stage of peptide microarray technology.

Overall, we successfully employed a peptide microarray-based tyrosine kinase activity screening technique, identifying new potential targets for pediatric brain tumor treatment. The obtained kinase activity profiles suggest the existence of a more tumor-specific kinase activity profile including CDK2 and c-Met, confirming earlier reports showing activation of these kinases. In the era of a rapidly increasing number of small-molecule inhibitors, this tyrosine kinase activity profiling method will be of tremendous value by enabling us to rapidly screen for potential druggable targets in a broad range of malignancies.

Disclosure of Potential Conflicts of Interest

No potential conflicts of interest were disclosed.

Acknowledgments

Received 9/19/08; revised 3/17/09; accepted 5/15/09; published OnlineFirst 6/30/09.

Grant support: Foundation of Pediatric Oncology Groningen grant SKOG-05-001 (A.H. Sikkema).

The costs of publication of this article were defrayed in part by the payment of page charges. This article must therefore be hereby marked *advertisement* in accordance with 18 U.S.C. Section 1734 solely to indicate this fact.

We thank Dr. Michael S. Bobola (Seattle Children's Hospital Research Institute) for making the pediatric brain tumor cell lines available.

References

1. Irish JM, Hovland R, Krutzik PO, et al. Single cell profiling of potentiated phospho-protein networks in cancer cells. Cell 2004;118:217–28.
2. Steelman LS, Pohnert SC, Shelton JG, Franklin RA, Bertrand FE, McCubrey JA. JAK/STAT, Raf/MEK/ERK, PI3K/Akt and BCR-ABL in cell cycle progression and leukemogenesis. Leukemia 2004;18:189–218.
3. Addo-Yobo SO, Straessle J, Anwar A, Donson AM, Kleinschmidt-DeMasters BK, Foreman NK. Paired overexpression of ErbB3 and Sox10 in pilocytic astrocytoma. J Neuropathol Exp Neurol 2006;65:769–75.
4. Gilbertson RJ, Bentley L, Hernan R, et al. ERBB receptor signaling promotes ependymoma cell proliferation and represents a potential novel therapeutic target for this disease. Clin Cancer Res 2002;8:3054–64.
5. Gilbertson RJ, Langdon JA, Hollander A, et al. Mutational analysis of PDGFR-RAS/MAPK pathway activation in childhood medulloblastoma. Eur J Cancer 2006;42:646–9.
6. Andrae J, Molander C, Smits A, Funa K, Nister M. Platelet-derived growth factor-B and -C and active α-receptors in medulloblastoma cells. Biochem Biophys Res Commun 2002;296:604–11.
7. Gilbertson RJ. Medulloblastoma: signalling a change in treatment. Lancet Oncol 2004;5:209–18.

8. Hartmann W, Digon-Sontgerath B, Koch A, et al. Phosphatidylinositol 3'-kinase/AKT signaling is activated in medulloblastoma cell proliferation and is associated with reduced expression of PTEN. Clin Cancer Res 2006;12:3019–27.
9. Shigaki S, Yamaji T, Han X, et al. A peptide microarray for the detection of protein kinase activity in cell lysate. Anal Sci 2007;23:271–5.
10. Diks SH, Kok K, O'Toole T, et al. Kinome profiling for studying lipopolysaccharide signal transduction in human peripheral blood mononuclear cells. J Biol Chem 2004;279:49206–13.
11. van Baal JW, Diks SH, Wanders RJ, et al. Comparison of kinome profiles of Barrett's esophagus with normal squamous esophagus and normal gastric cardia. Cancer Res 2006;66:11605–12.
12. Brueggemeier SB, Wu D, Kron SJ, Palecek SP. Protein-acrylamide copolymer hydrogels for array-based detection of tyrosine kinase activity from cell lysates. Biomacromolecules 2005;6:2765–75.
13. Houseman BT, Huh JH, Kron SJ, Mrksich M. Peptide chips for the quantitative evaluation of protein kinase activity. Nat Biotechnol 2002;20:270–4.
14. Lemeer S, Jopling C, Naji F, et al. Protein-tyrosine kinase activity profiling in knock down zebrafish embryos. PLoS ONE 2007;2:e581.
15. Louis DN, Ohgaki H, Wiestler OD, Cavenee WK. WHO classification of the central nervous system. 4th ed. Lyon: IARC; 2007.
16. Diks SH, Hardwick JC, Diab RM, et al. Activation of the canonical β-catenin pathway by histamine. J Biol Chem 2003;278:52491–6.
17. Kinoshita E, Kinoshita-Kikuta E, Takiyama K, Koike T. Phosphate-binding tag, a new tool to visualize phosphorylated proteins. Mol Cell Proteomics 2006;5:749–57.
18. Wright GW, Simon RM. A random variance model for detection of differential gene expression in small microarray experiments. Bioinformatics 2003;19:2448–55.
19. Diks SH, Parikh K, van der SM, Joore J, Ritsema T, Peppelenbosch MP. Evidence for a minimal eukaryotic phosphoproteome? PLoS ONE 2007;2:e777.
20. Roskoski R, Jr. Src protein-tyrosine kinase structure and regulation. Biochem Biophys Res Commun 2004;324:1155–64.
21. Sun G, Sharma AK, Budde RJ. Autophosphorylation of Src and Yes blocks their inactivation by Csk phosphorylation. Oncogene 1998;17:1587–95.
22. Fiskus W, Pranpat M, Balasis M, et al. Cotreatment with vorinostat (suberoylanilide hydroxamic acid) enhances activity of dasatinib (BMS-354825) against imatinib mesylate-sensitive or imatinib mesylate-resistant chronic myelogenous leukemia cells. Clin Cancer Res 2006;12:5869–78.
23. Li J, Wang Y, Sun Y, Lawrence TS. Wild-type TP53 inhibits G(2)-phase checkpoint abrogation and radiosensitization induced by PD0166285, a WEE1 kinase inhibitor. Radiat Res 2002;157:322–30.
24. Rowley R, Hudson J, Young PG. The wee1 protein kinase is required for radiation-induced mitotic delay. Nature 1992;356:353–5.
25. Wang Y, Decker SJ, Sebolt-Leopold J. Knockdown of Chk1, Wee1 and Myt1 by RNA interference abrogates G_2 checkpoint and induces apoptosis. Cancer Biol Ther 2004;3:305–13.
26. Colozza M, Azambuja E, Cardoso F, Sotiriou C, Larsimont D, Piccart MJ. Proliferative markers as prognostic and predictive tools in early breast cancer: where are we now? Ann Oncol 2005;16:1723–39.
27. Muller-Tidow C, Metzger R, Kugler K, et al. Cyclin E is the only cyclin-dependent kinase 2-associated cyclin that predicts metastasis and survival in early stage non-small cell lung cancer. Cancer Res 2001;61:647–53.
28. Lamszus K, Schmidt NO, Jin L, et al. Scatter factor promotes motility of human glioma and neuromicrovascular endothelial cells. Int J Cancer 1998;75:19–28.
29. Schmidt NO, Westphal M, Hagel C, et al. Levels of vascular endothelial growth factor, hepatocyte growth factor/scatter factor and basic fibroblast growth factor in human gliomas and their relation to angiogenesis. Int J Cancer 1999;84:10–8.
30. Birchmeier C, Birchmeier W, Gherardi E, Vande Woude GF. Met, metastasis, motility and more. Nat Rev Mol Cell Biol 2003;4:915–25.
31. Abounader R, Lal B, Luddy C, et al. *In vivo* targeting of SF/HGF and c-met expression via U1snRNA/ribozymes inhibits glioma growth and angiogenesis and promotes apoptosis. FASEB J 2002;16:108–10.
32. Li Y, Lal B, Kwon S, et al. The scatter factor/hepatocyte growth factor: c-met pathway in human embryonal central nervous system tumor malignancy. Cancer Res 2005;65:9355–62.
33. Gilbertson RJ, Perry RH, Kelly PJ, Pearson AD, Lunec J. Prognostic significance of HER2 and HER4 coexpression in childhood medulloblastoma. Cancer Res 1997;57:3272–80.
34. Bodey B, Kaiser HE, Siegel SE. Epidermal growth factor receptor (EGFR) expression in childhood brain tumors. *In Vivo* 2005;19:931–41.
35. Thomas SM, Brugge JS. Cellular functions regulated by Src family kinases. Annu Rev Cell Dev Biol 1997;13:513–609.
36. Finn RS, Dering J, Ginther C, et al. Dasatinib, an orally active small molecule inhibitor of both the src and abl kinases, selectively inhibits growth of basal-type/"triple-negative" breast cancer cell lines growing *in vitro*. Breast Cancer Res Treat 2007;105:319–26.
37. Johnson FM, Saigal B, Talpaz M, Donato NJ. Dasatinib (BMS-354825) tyrosine kinase inhibitor suppresses invasion and induces cell cycle arrest and apoptosis of head and neck squamous cell carcinoma and non-small cell lung cancer cells. Clin Cancer Res 2005;11:6924–32.
38. Timeus F, Crescenzio N, Fandi A, Doria A, Foglia L, Cordero di ML. *In vitro* antiproliferative and antimigratory activity of dasatinib in neuroblastoma and Ewing sarcoma cell lines. Oncol Rep 2008;19:353–9.
39. Lombardo LJ, Lee FY, Chen P, et al. Discovery of *N*-(2-chloro-6-methyl-phenyl)-2-(6-(4-(2-hydroxyethyl)-piperazin-1-yl)-2-methylpyrimidin-4-ylamino)thiazole-5-carboxamide (BMS-354825), a dual Src/Abl kinase inhibitor with potent antitumor activity in preclinical assays. J Med Chem 2004;47:6658–61.
40. Fults DW, Towle AC, Lauder JM, Maness PF. pp60c-src in the developing cerebellum. Mol Cell Biol 1985;5:27–32.
41. Nishihara E, Yoshida-Komiya H, Chan CS, et al. SRC-1 null mice exhibit moderate motor dysfunction and delayed development of cerebellar Purkinje cells. J Neurosci 2003;23:213–22.
42. Kuo G, Arnaud L, Kronstad-O'Brien P, Cooper JA. Absence of Fyn and Src causes a reeler-like phenotype. J Neurosci 2005;25:8578–86.
43. Kleber S, Sancho-Martinez I, Wiestler B, et al. Yes and PI3K bind CD95 to signal invasion of glioblastoma. Cancer Cell 2008;13:235–48.
44. Park CM, Park MJ, Kwak HJ, et al. Ionizing radiation enhances matrix metalloproteinase-2 secretion and invasion of glioma cells through Src/epidermal growth factor receptor-mediated p38/Akt and phosphatidylinositol 3-kinase/Akt signaling pathways. Cancer Res 2006;66:8511–9.
45. Dey N, Crosswell HE, De P, et al. The protein phosphatase activity of PTEN regulates SRC family kinases and controls glioma migration. Cancer Res 2008;68:1862–71.
46. Porkka K, Koskenvesa P, Lundan T, et al. Dasatinib crosses the blood-brain barrier and is an efficient therapy for central nervous system Philadelphia chromosome-positive leukemia. Blood 2008;112:1005–12.
47. Lemeer S, Ruijtenbeek R, Pinkse MW, et al. Endogenous phosphotyrosine signaling in zebrafish embryos. Mol Cell Proteomics 2007;6:2088–99.